Quantitative interpretation sensitivity to angle and frequency-dependent pre-stack time shift, amplitude and phase perturbations

Matthew Whaley[1], Cyrille Reiser[1] and Andrew Long[1*] present a modelling study to quantify how angle-dependent time shifts, angle-dependent frequency variations, or frequency-dependent phase errors can impact the recovery of elastic impedance attributes using pre-stack simultaneous seismic inversion.

Introduction

As discussed by Long (2017), marine 'broadband' signal processing flows typically incorporate a combination of free-surface deghosting, spectral shaping, and attenuation compensation. Overall, there are many opportunities to corrupt the phase content in an angle-dependent and frequency-dependent manner during any signal processing flow, and such risks may increase during aggressive 'broadband' flows.

We conducted a synthetic modelling study to quantify and understand how angle-dependent time shifts, angle-dependent frequency variations, or frequency-dependent phase errors can impact the recovery of elastic impedance attributes using pre-stack simultaneous seismic inversion. All modelling and inversion was 2D in nature, included no noise considerations, and assumed the velocity model was perfectly understood.

Modelling methodology

An assessment of any 'broadband' seismic dataset will be more qualitative when judging post-stack data (SNR, resolution, whether events seem zero phase, etc.) and more quantitative pre-stack courtesy of AVA and well-tie analyses (phase stability, angle-dependent well ties, bandwidth, elastic cross-plot analyses,

etc.). Of particular relevance to the discussion here is that the effects of frequency-dependent phase rotations may be difficult to observe on post-stack images, often being inseparable from time shifts or time dilations, whereas the pre-stack effects are more easily observable and quantifiable. It is very challenging to reliably establish that a dataset is precisely zero phase. However, anecdotally we observe that most seismic datasets (whether conventional or broadband) after zero phase corrections during signal processing tend to be within about 30° of true zero phase when compared to a reliable well-to-seismic tie. Subjectively, we typically see that phase errors of this magnitude have little or no discernible effects upon post-stack mapping and interpretation of stacked reflectivity data (refer to the upper row of Figure 1). However, the effect of phase rotations with the same magnitude on pre-stack data prior to AVA studies or inversion can be far more significant – for example, the AVA Gradient in the lower row of Figure 1. Note that the Gradient in each panel in the lower row of Figure 1 was estimated by using a two-term Shuey approximation, and the inputs were the (perturbed) far angle stack in the panel above it along with unperturbed near angle stacks.

Several North Sea wells were used to build realistic 2D earth models (Figure 2) with high resolution stratigraphic detail.
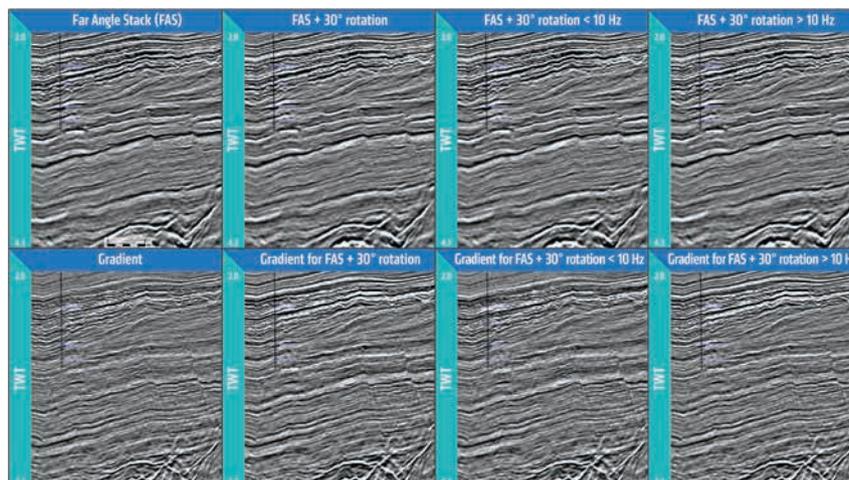
Figure 1 From left to right, far angle stack, far angle stack + 30° phase rotation for all frequencies, far angle stack + 30° phase rotation for 0-10 Hz, and far angle stack + 30° phase rotation for 10-125 Hz. (upper) Far angle (reflectivity) stack (FAS), and (lower) AVA Gradient computed using the (perturbed) FAS result above it. Phase rotations of 30° are not easily evident on reflectivity stacks, but noticeable differences are evident when the AVA Gradient is calculated using a far angle stack with these phase errors.

[1] PGS
[*] andrew.long@pgs.com
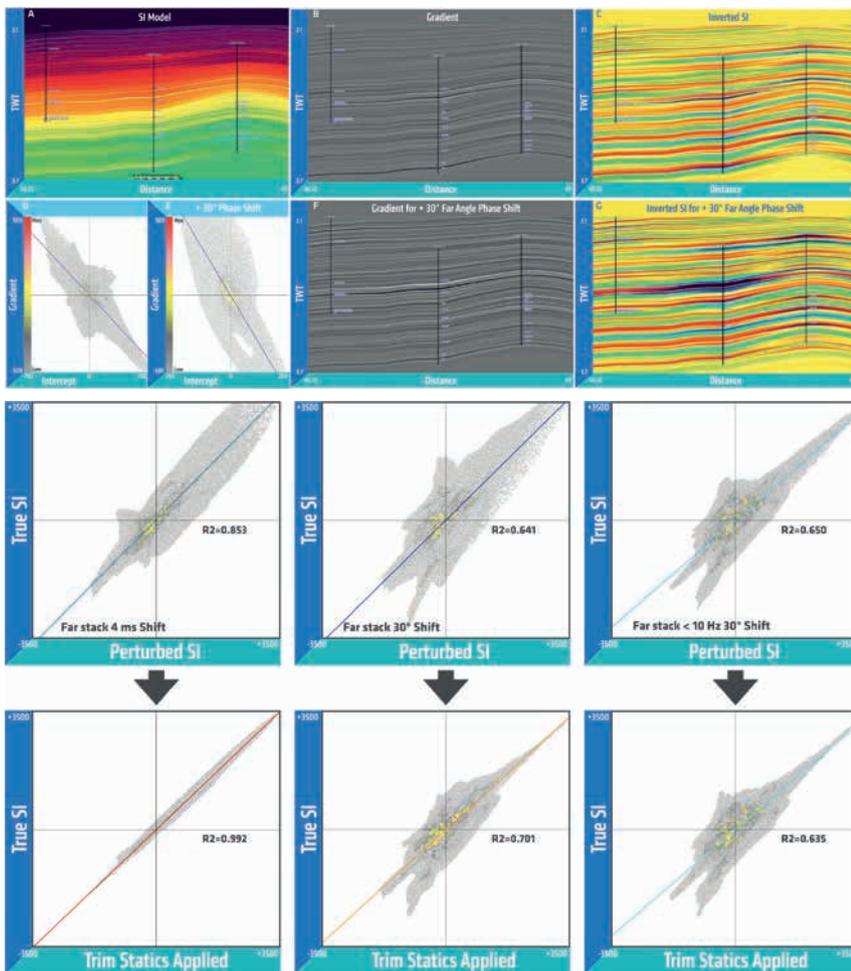
Figure 2 (A) Reference synthetic earth model (colour = Shear Impedance: SI); (B) Gradient from synthetic stacks; (C) Inversion of Shear Impedance using synthetic stacks; (D,E) Intercept-Gradient cross-plots before and after +30° phase rotation of all far angle stack frequencies; (F) Gradient from synthetic stacks after +30° phase rotation of all far angle stack frequencies; (G) Inversion of Shear Impedance using synthetic stacks after +30° phase rotation of all far angle stack frequencies.

Figure 3 Cross-plots of the model Shear Impedance (vertical axes) and perturbed Shear Impedance (horizontal axes) for perturbations of (left) +4 ms time shift applied to the far angle stack, (center) 30° phase shift applied to all frequencies of the far angle stack, and (right) 30° phase shift applied to all frequencies <10 Hz of the far angle stack. In each scenario trim statics have been applied (lower row) in an effort to mitigate the effects of the perturbation. The coefficient of determination between the two datasets in each panel is also annotated.

A broadband wavelet was extracted from real dual-sensor broadband data and convolved with the earth models to produce near, mid and far angle stacks using the Shuey two-term AVA approximation (Shuey, 1985). These three angle stacks were then inverted using simultaneous pre-stack inversion to estimate Intercept (I), Gradient (G), Acoustic Impedance (AI), Shear Impedance (SI), and the Vp/Vs ratio. Time shifts, low and high frequency spectral slope variations, and frequency-dependent phase rotations were then applied to the far angle stack as follows: a time shift of +4 ms, +30° phase rotation to frequencies < 10 Hz, +30° phase rotation frequencies > 10 Hz, and +30° phase rotation to all frequencies. Angle-dependent frequency filters were also applied to the data as follows: 1. Hi-cut variations courtesy of a 20-90 Hz hi-cut applied to the mid angle stack and a 10-60 Hz hi-cut applied to the far angle stack, and 2. Lo-cut variations courtesy of a 3-9 Hz lo-cut applied to the near angle stack, a 3-7 Hz lo-cut applied to the mid angle stack a 3-5 Hz lo-cut applied to the far angle stack. Two types of simple mitigation were also attempted after each perturbation; either the application of trim statics (residual angle stack mis-alignment) corrections or the application of offset-dependent spectral corrections (ODSC) to balance the amplitude spectra across all angles.

Various analyses were then performed using frequency spectra and elastic attribute cross-plots to assess the sensitivity of Quantitative Interpretation (QI) to the various perturbations. Table 1 summarizes the overall findings. Our ambition through-

out was to use simple and robust QC procedures that would be applicable in real world settings.

Analysis of modelling results

As evident in Table 1, the most sensitive parameters to the perturbations tested were the Gradient, Shear Impedance, and the Vp/Vs ratio. Time shift errors have the greatest effect upon the Gradient; low frequency phase errors and angle-dependent low frequency spectral slope variations have the greatest effect upon the estimated Shear Impedance; and the estimated Vp/Vs ratio is sensitive to everything — most notably far angle phase rotation (all frequencies), low frequency phase rotation of the far angle stack, and time shifts applied to the far angle stack. While the effects of time shifts can be mitigated in processing with high success using trim statics corrections, the effects of phase rotations upon Shear Impedance and Vp/Vs estimation remained severe after both trim statics or ODSC corrections. It is unsurprising that both the Intercept and Acoustic Impedance estimation are largely unaffected as they should be less dependent on mid-angle and far-angle perturbations. Correspondingly, it also follows that perturbations of far angle stack data should have the greatest effect upon the estimated Shear Impedance and Vp/Vs ratio — as observed. High frequency phase rotations act in similar ways to angle-dependent time shifts, and, along with angle-dependent high frequency slope variations, were generally mitigated successfully. Collectively, the sensitivity tests discussed

here form a useful reference for real broadband data QC, and identify which problems are more easily mitigated. We acknowledge that the synthetic data used were noise-free and unaffected by wavelet stretch.

The top row of Figure 3 reinforces the similar effects of far angle time shifts and phase rotations when cross-plotting estimated versus true Shear Impedance. The application of trim statics (lower row) mitigates the effects of time shifts, but not the effects of phase rotations. Note that a constant phase rotation incurs an increasingly larger time shift at lower frequencies.

In Figure 4 the mid angle stack had a 20-90 Hz hi-cut frequency filter applied, and the far angle stack had a 10-60 Hz hi-cut frequency filter applied, simulating an increasingly severe loss of high frequency content with increasing angle — clearly evident in the upper-left panel. There is also a clear difference in the relative Intercept and Gradient amplitudes towards higher frequencies in the upper-centre panel. Interestingly, the Intercept-Gradient cross-plots show that the I-G trend becomes steeper and the attributes are more highly correlated when there are high frequency spectra differences. By comparison, when

the angle-dependent frequency spectra are matching (lower-left panel) and the Intercept and Gradient frequency spectra are more comparable (lower-centre panel), the I-G distribution is less correlated (lower-right panel). Furthermore, Table 1 shows that the Gradient value has a coefficient of determination of 0.79 before ODSC, and 0.98 after ODSC application.

In Figure 5 a 3-9 Hz lo-cut frequency filter was applied to the near angle stack, a 3-7 Hz lo-cut frequency filter was applied to the mid angle stack, and a 3-5 Hz lo-cut frequency filter was applied to the far angle stack, simulating an increasingly severe loss of low frequency content with decreasing angle. Overall, apart from rather subtle low frequency differences between the angle-dependent spectra (upper-left panel) and the Intercept and Gradient spectra (upper-centre panel), these errors are not easily detectable. The application of ODSC induces relatively little effect upon the Intercept-Gradient cross-plots, and the I-G trend is relatively unchanged (see also Table 1). However, the statistical errors in the Shear Impedance and Vp/Vs ratio introduced by the angle-dependent low-frequency amplitude mismatch are significant (R^2 values of 0.36 and 0.67, respectively, in Table 1)

	Original Synthetic	Far stack + 4ms time shift	Apply Trim Statics	Far stack + 30° phase shift	Apply Trim Statics	Far stack + 30° phase shift < 10 Hz	Apply Trim Statics	Far stack + 30° phase shift > 10 Hz	Apply Trim Statics	Mid stack 20-90 Hz hi-cut, Far stack 10-60 Hz hi-cut	Apply ODSC	Near stack 3-9 Hz lo-cut, Mid stack 3-7 Hz lo-cut, Far stack 3-5 Hz lo-cut	Apply ODSC
I	1	0.98	1	0.99	0.99	1	1	0.99	1	1	1	0.97	0.98
G	1	0.43	0.97	0.74	0.8	0.87	0.86	0.82	0.91	0.79	0.98	0.9	0.95
AI	1	0.99	1	0.99	0.99	0.99	0.99	1	1	1	1	0.88	0.94
SI	1	0.85	0.99	0.64	0.7	0.65	0.64	0.88	0.96	0.95	0.99	0.36	0.88
Vp/Vs	1	0.53	0.97	0.33	0.49	0.35	0.36	0.76	0.89	0.77	0.99	0.67	0.9

Table 1 Summary of time shift and phase shift perturbations applied to the synthetic data. In each cell the number represents the coefficient of determination (R^2) between the reference (unperturbed) model and the perturbed result, with and without efforts to mitigate the associated errors (pairs of columns representing each perturbation and its mitigation). The most significant errors are associated with phase shifts, followed by angle-dependent variations in low frequency content, followed by angle-dependent variations in high frequency content.
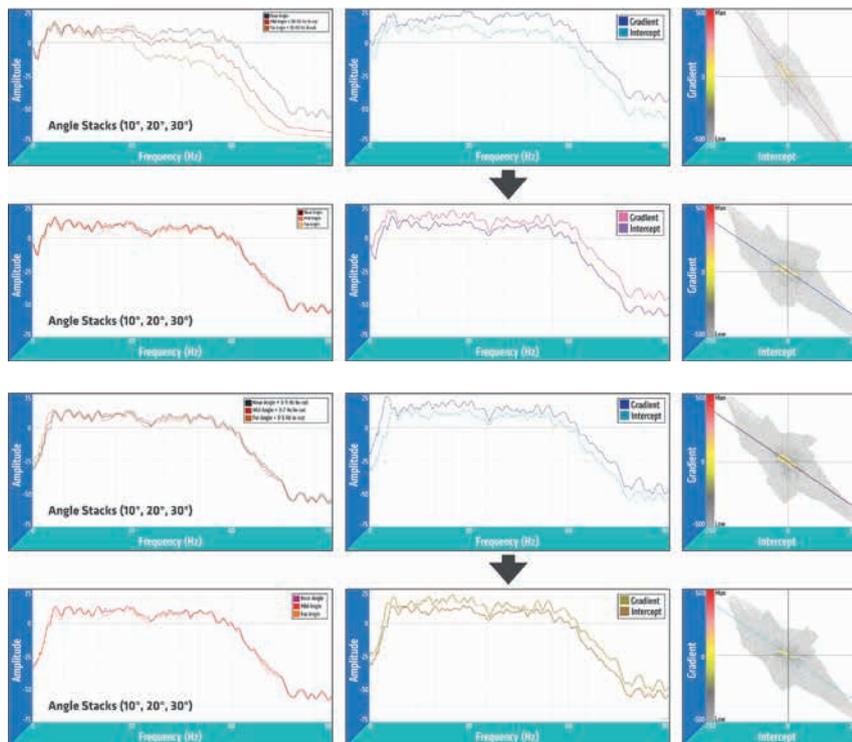
Figure 4 Frequency spectra of near, mid and far angle stacks after angle-dependent hi-cut frequency filtering (left); associated Intercept and Gradient stacks (centre); and the associated Intercept-Gradient cross-plots (right), before (upper row) and after (lower row) ODSC corrections. Refer also to Figure 6.

Figure 5 Frequency spectra of near, mid and far angle stacks after angle-dependent lo-cut frequency filtering (left); associated Intercept and Gradient stacks (centre); and the associated Intercept-Gradient cross-plots (right), before (upper row) and after (lower row) ODSC corrections. Refer also to Figure 6.
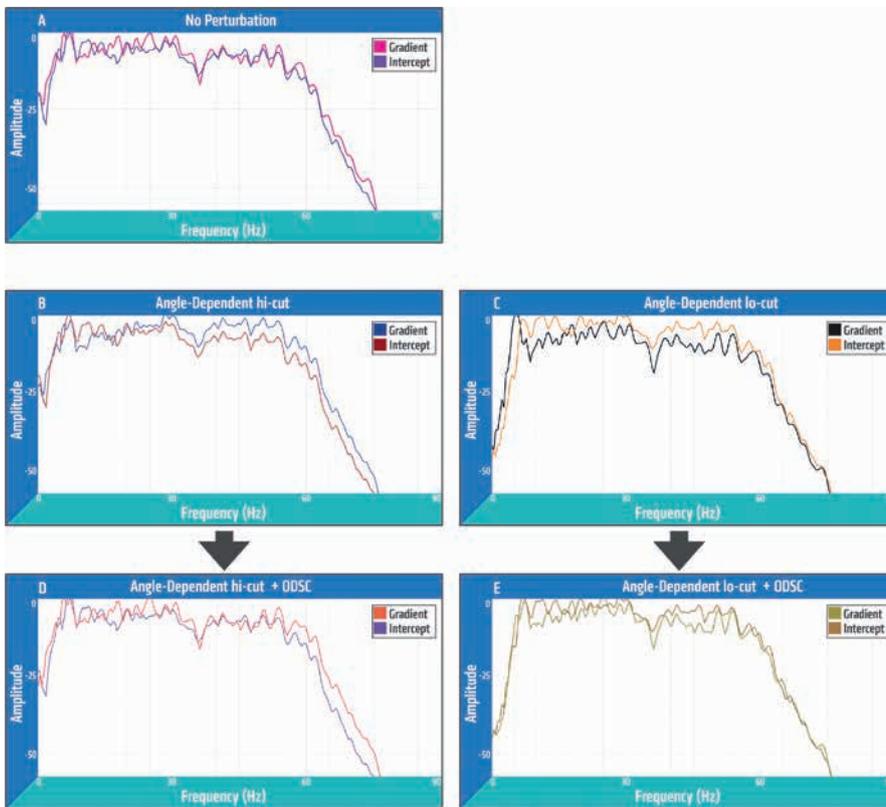
Figure 6 Normalized amplitude spectra for Intercept and Gradient results. (A) unperturbed model; (B) angle-dependent high frequency mismatch before ODSC; (C) angle-dependent low frequency mismatch before ODSC; (D) angle-dependent high frequency mismatch after ODSC; and (E) angle-dependent low frequency mismatch after ODSC.

despite not being visually evident in the I-G cross-plots before or after ODSC application in Figure 5.

Figure 6 shows that careful inspection of normalized Intercept and Gradient spectra may indicate the presence of angle-dependent high frequency variations in the input angle stacks; expressed as an overall amplitude difference at higher frequencies and a correlated spectral shape that is unrealistic (Figure 6b). The application of ODSC removes the correlation in spectral shape with reasonable success (Figure 6d). It is more difficult to detect the presence of angle-dependent low frequency variations in the input angle stacks by examination of normalized Intercept and Gradient spectra, apart from a frequency shift of the first peak (Figure 6c), and again the application of ODSC is reasonably successful (Figure 6e).

Summary

The simple synthetic data analyses presented here highlight some pitfalls when attempting to QC seismic data being used for pre-stack inversion. For example, the detection of angle-dependent low frequency amplitude variations may be difficult as they are not apparent on either frequency spectra or cross-plots of Intercept and Gradient data. Angle-dependent time shifts or high frequency variations tend to have similar expressions upon inversion results. The most serious problems arise due to angle-dependent low frequency phase errors: significant errors in the estimated Shear

Impedance and Vp/Vs ratio cannot be mitigated by trim statics or ODSC application, and the estimated Gradient error may also be moderately large. Angle-dependent variations in low frequency content (with no phase or time shift errors) can also create significant errors in the estimated Shear Impedance and Vp/Vs ratio, and may not be detectable on Intercept-Gradient cross-plots before or after ODSC application.

Overall, these results reinforce motivations to pursue broadband pre-stack processing solutions (free-surface deghosting, spectral shaping, and attenuation compensation) that are as deterministic and predictable as possible, and less likely to introduce statistical variability in angle-dependent and/or frequency-dependent phase shifts that are clearly easy to overlook even on noise-free data such as the synthetics considered here.

References

Long, A. [2017]. A bigger picture view of separated wavefields and marine broadband seismic. *First Break*, **35** (6), 81-86.

Shuey, R.T. [1985]. A simplification of the Zoeppritz equations. *Geophysics*, **50** (4), 609-614.